DOI: 10.1002/chem.200701364

Interpenetrated Three-Dimensional $Mn^{II}M^{III}$ Ferrimagnets, $[Mn(4dmap)_4]_3[M(CN)_6]_2 \cdot 10H_2O$ (M = Cr, Mn): Structures, Magnetic Properties, and Pressure-Responsive Magnetic Modulation

Wakako Kaneko,[a] Masaki Mito,[b] Susumu Kitagawa,*[a] and Masaaki Ohba*[a]

Abstract: Two novel cyanide-bridged ferrimagnets, $[Mn(4dmap)_4]_3[M(CN)_6]_2 \cdot 10H_2O$ (4dmap = 4-dimethylaminopyridine, M = Cr (**1**) and Mn (**2**)), have been prepared from the reaction of $MnCl_2 \cdot 4H_2O$, a monodentate coligand (4dmap), with $K_3[M(CN)_6]$. X-ray crystallographic results show that these are isomorphous, and form a unique twofold interpenetrated three-dimensional framework with a triconnected 6.10^2 net. The framework contains two types of one-dimensional channel: hexagonal channels based on a cyanide-bridged Mn_6M_6 hexagon, and triangle channels segmented by CN-Mn-NC linkages, which are filled with lattice water molecules. The dimethylamino groups of the 4dmap coligands are located around a pore and form the basic inner space. Variable-temperature X-ray powder diffraction and thermogravimetric analysis results show that the frameworks of both compounds are susceptible to dehydration through the loss of strongly hydrogen-bonded lattice water molecules. Magnetic measurements on both compounds show a ferrimagnetic ordering occurs at low temperature, $T_C = 17$ K for **1** and 6 K for **2**. Application of hydrostatic pressure showed a positive effect on the magnetic ordering. Both values of T_C increased linearly, to 25 K for **1** and 15 K for **2** at 1.0 GPa. The magnetic properties of both compounds were reversibly modulated by the external stress.

Keywords: chromium · ferrimagnet · interpenetrated frameworks · manganese · pressure-responsive magnetism

Introduction

The diversity of frameworks is one of the most representative features of coordination polymers. The attainment of multiple functions providing interlocking, coexistence or control of magnetism, optical properties, ferroelectricity, conductivity, and gas adsorption, is an attractive topic in the field of material chemistry, in which coordination polymer frameworks are expected to be platforms for such multifunctionality.[1–5] The characteristics of coordination polymers are summarized as: 1) the chemical multiplicity of the constitutive metal ions and ligands; 2) a designable and regular framework based on the intrinsic topology of the constituents; and 3) a flexible framework based on the coordination bonds.[6] These characteristics enable us to provide desirable materials based on coordination polymers by the modification of the constituents using rational design. In particular, the flexible framework allows responsivity to external physical and/or chemical stimuli (e.g., pressure, light, temperature, and guest molecules). These structural changes usually lead to changes in the compounds′ physical properties. For example, coordination polymer magnets (CPMs), also called molecule-based magnets, sensitively respond to such structural changes, because structural perturbations directly affect the local overlap integral of their magnetic orbitals (i.e., magnetic interaction), which is reflected in the magnetic properties in the bulk.[7–21] Above all, the structural flexibility of coordination polymers is expected to be crucial for multifunctionality based on a physical and/or chemical response.

A large number of Prussian blue-inspired compounds—more specifically, cyanide-bridged bimetallic assemblies—consisting of hexacyanometalate building units,

[a] W. Kaneko, Prof. S. Kitagawa, Dr. M. Ohba
Department of Synthetic Chemistry and Biological Chemistry
Graduate School of Engineering, Kyoto University
Katsura, Nishikyo-ku, Kyoto 615–8510 (Japan)
Fax: (+75) 383-2732
E-mail: ohba@sbchem.kyoto-u.ac.jp

[b] Dr. M. Mito
Department of Electronics, Faculty of Engineering
Kyushu Institute of Technology
Sensui-cho, Tobata-ku, Kitakyushu, 804–8550 (Japan)

Supporting information for this article is available on the WWW under http://www.chemeurj.org/ or from the author.

$[M_A(CN)_6]^{3-}$, and cationic compounds, $[M_B(L)_n]^{n+}$ (L = organic co-ligand), have been widely investigated to date.[22–25] Most of these show ordered magnetism (ferromagnetism, ferrimagnetism, and metamagnetism) with a multidimensional framework, and are classified as CPMs. We have been studying the systematic synthesis, crystal structures, and magnetic and magneto-optical properties of CPMs, and have managed to control their magnetism using an external stimulus such as hydrostatic pressure and/or guest molecules.[11,14,20,21,24–31] The pressure responsivity is driven by the flexibility of the M_A-CN-M_B linkages and the internetwork space. Low-dimensional frameworks allow marked magnetic conversions on application of weaker external stimuli because of the internet interactions. However, such internet interactions are disadvantageous for the long-range magnetic ordering in the bulk, and their natures fluctuate between ferromagnetic and antiferromagnetic depending on the distance between the neighboring networks.[11,12] On the other hand, a three-dimensional (3D) framework composed of a large number of connecting nodes, n (e. g., $n_{max.}=6$ for $[M_A(CN)_6]^{3-}$ in face-centered-cubic structure), is advantageous for magnetic ordering.[32,33] In addition, 3D CPMs with a small number of n are more advantageous for reversible response to external pressure due to their structural flexibility. In consideration of these aspects, interpenetrated 3D frameworks can combine the assets of low- and high-dimensional frameworks, and are expected to exhibit strong 3D magnetic interactions and dynamic structural flexibility.[33–35] The key for acquiring such a convertible structure is to construct an interior void space in a CPM with weak internet interactions, such as π–π stacking and hydrogen bonds. In regard to 3D interpenetrated CPMs, a relatively bulky pyridine-derivative coligand would favor providing a spatial margin and weak internet interaction between the frameworks, in which the porosity and the interpenetrated framework are regarded as devices equipped to respond to chemical and physical stimuli, respectively. There are few examples of such 3D interpenetrated CPMs, and systematic studies on the effect of pressure on CPMs have not been carried out because of the lack of suitable compounds.

Here, we report on the structures and magnetic properties of a new type of cyanide-bridged $Mn^{II}M^{III}$ ferrimagnet; $[Mn(4dmap)_4]_3[M(CN)_6]_2\cdot 10H_2O$ (M = Cr (**1**) and Mn (**2**)). Compounds **1** and **2** are isomorphous and form a unique twofold interpenetrated 3D network with a triconnected 6.10^2 net consisting of M^{III} ions as nodes ($n=3$) and CN-Mn-NC units as linkers. The magnetic characteristics, which are dependent on the constituent M^{III} ions, and a reversible pressure effect are well demonstrated.

Results and Discussion

Preparation: $[Mn(4dmap)_4]_3[M(CN)_6]_2\cdot 10H_2O$ (M = Cr (**1**) and Mn (**2**)) were obtained as pale green (**1**) and reddish-brown (**2**) cubic crystals from the reaction of $MnCl_2\cdot 4H_2O$, 4dmap, and $K_3[M(CN)_6]$ in a deoxygenated water–ethanol mixture (2:1) in a molar ratio of 3:18:2 at room temperature for **1**, and in deoxygenated water in a molar ratio of 3:12:2 at 276 K for **2** (see Figure S1 in the Supporting Information). The cold conditions were essential for the synthesis of **2**, because $K_3[Mn(CN)_6]$ decomposes readily in H_2O, even at room temperature.[31] These compounds showed two ν(C≡N) bands at 2156 and 2131 cm^{-1} for **1**, and four ν(C≡N) bands at 2141, 2135, 2120, and 2118 cm^{-1} for **2**, indicating the existence of bridging and terminal cyanide groups in their structures.[36–39]

In previous cyanide-bridged CPs, much effort was devoted to obtain single crystals suitable for structural determination by using various chelate coligands (L), such as ethylenediamine (bidentate), diethylenetriamine (tridentate), and their derivatives, in which the slow dissociation of the coligands from a precursor ML_n avoided any immediate precipitation of a by-product $M_{B3}[M_A(CN)_6]_2\cdot nH_2O$.[24,25] In this synthesis, we used the monodentate coligand, 4dmap, which is not convenient for reaction with Mn^{II} ions, because 4dmap does not evoke stabilization energy from the chelate effect and so the Mn^{II} ion (d^5, high spin) gains no ligand field stabilization energy (LFSE) from complexation. In spite of such a disadvantage, the use of 4dmap enables us to obtain suitable crystals of $Mn^{II}M^{III}$ compounds in good yields. The X-ray crystal structures revealed that C–H···π contacts formed between the basic dimethylamino group and the pyridine ring of 4dmap enable the formation of the framework.

Crystal structures: The X-ray crystal structure of **1** and **2** shows that they are isostructural, except for the different $[M(CN)_6]^{3-}$ unit (M = Cr (**1**) and Mn (**2**)). Hereafter, the structure of **1** is discussed as being representative of both structures (see Figure S2 and S3 in the Supporting Information for **2**). The asymmetric unit of **1** consists of one $[Mn1(4dmap)_4]^{2+}$ unit, one half of a $[Mn2(4dmap)_4]^{2+}$ unit, one $[Cr(CN)_6]^{3-}$ ion, and five lattice water molecules (Figure 1). The $[Cr(CN)_6]^{3-}$ bridges to two adjacent Mn1 atoms and one Mn2 atom in meridional mode. The Mn2 atom is located at an inversion center. Both Mn1 and Mn2 atoms are in a pseudo-octahedral geometry, surrounded by the four pyridine nitrogen atoms of the four 4dmap molecules (N7, N9, N11, and N13 for Mn1; N15, N17, $N15^{\#2}$, and $N17^{\#2}$ for

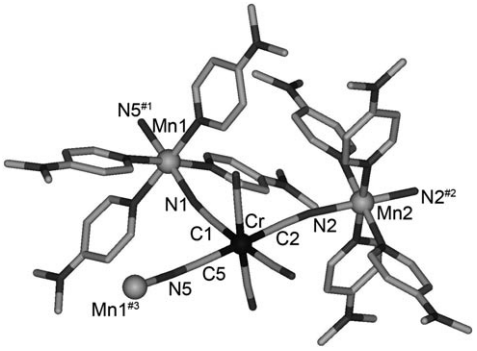

Figure 1. Basic structure of $[Mn(4dmap)_4]_3[Cr(CN)_6]_2\cdot 10H_2O$ (**1**). Hydrogen atoms and lattice water molecules are omitted for clarity.

Mn2) in the equatorial positions, and two cyanide nitrogen atoms of the $[Cr(CN)_6]^{3-}$ units (N1 and N5$^{\#1}$ for Mn1, and N2 and N2$^{\#2}$ for Mn2) at the axial positions. (The numerals #1 and #2 denote the symmetry operations of $(y, -x+y+1/3, -z+1/3)$ and $(-x, -y+1, -z+1)$, respectively.) The Mn1–N1, Mn1–N5$^{\#1}$, and Mn2–N2 bond lengths were 2.207(3), 2.216(3), and 2.194(3) Å, respectively. The Mn1-N1-C1, Mn1$^{\#3}$-N5-C5, and Mn2-N2-C2 bond angles were 168.4(3), 161.8(3), and 168.6(3)°, respectively, (where #3 = $(x-y+2/3, x+1/3, -z+1/3)$). The Cr-CN-Mn1-NC- linkages form a $Mn1_6Cr_6$ cyclohexane-type hexagon extended along the *ab* plane (Figure 2).

In the crystal lattice, the hexagons are connected by CN-Mn2-NC linkages, and a 3D coordination framework is formed that is represented as a triconnected $6,10^2$ net with the Cr^{III} ions acting as triconnected nodes and the -CN-Mn-NC- linkages as linkers (Figure 3).[40] Two individual $6,10^2$ nets are aligned parallel and twofold interpenetrated, with the hexagon units of each framework being alternately aligned along the *c* axis with intranet π–π interactions (C25···C38$^{\#2}$ = 3.461 Å). Narrow one-dimensional hexagonal and trigonal channels are formed along the *c* axis. The basic dimethylamino groups of 4dmap are located inside both channels, and the lattice water molecules are captured in these channels. The lattice water molecules are disordered in these channels, and form plural hydrogen bonds with each other and with the coordination-free cyanide nitrogen atoms of the host framework (N3, N4, and N6). A pyridine group of the 4dmap molecule on the $[Mn1(4dmap)_4]^{2+}$ unit forms contacts with a methyl group of the 4dmap molecule on another $[Mn1(4dmap)_4]^{2+}$ unit (C12–H5···C7$^{\#4}$ = 2.783 Å and C20–H18···C25$^{\#5}$ = 2.758 Å, #4 = $(y+2/3, x+1/3, -z+1/3)$ and #5 = $(-x, -y+1, -z)$), which also contributes to the framework formation based on the intranet CH···π interactions. The shortest internet Mn1···Cr, Mn2···Cr, Cr···Cr, Mn1···Mn1, Mn2···Mn2, and Mn1···Mn2 distances were 10.917, 11.265, 10.646, 11.890, 13.121, and 14.467 Å, respectively, for **1**. Taking the van der Waals radii into consideration, the guest accessible volume of both **1** and **2** was estimated to be about 6.7%, without any lattice water molecules being present.[41]

Framework stability: To examine the structural stability of **1** and **2** towards dehydration, we carried out thermogravimetric analysis (TGA) and measurements on the thermal dependence of the X-ray powder diffraction (XRPD) patterns. The TGA data of both compounds showed a rapid and continuous loss of weight on heating (Figure 4). Compound **1** lost all its lattice water molecules at 370 K, and then decomposed in stages. In contrast, compound **2** lost all its lattice water molecules at 370 K, and then immediately decomposed. Both these results suggest each framework had ther-

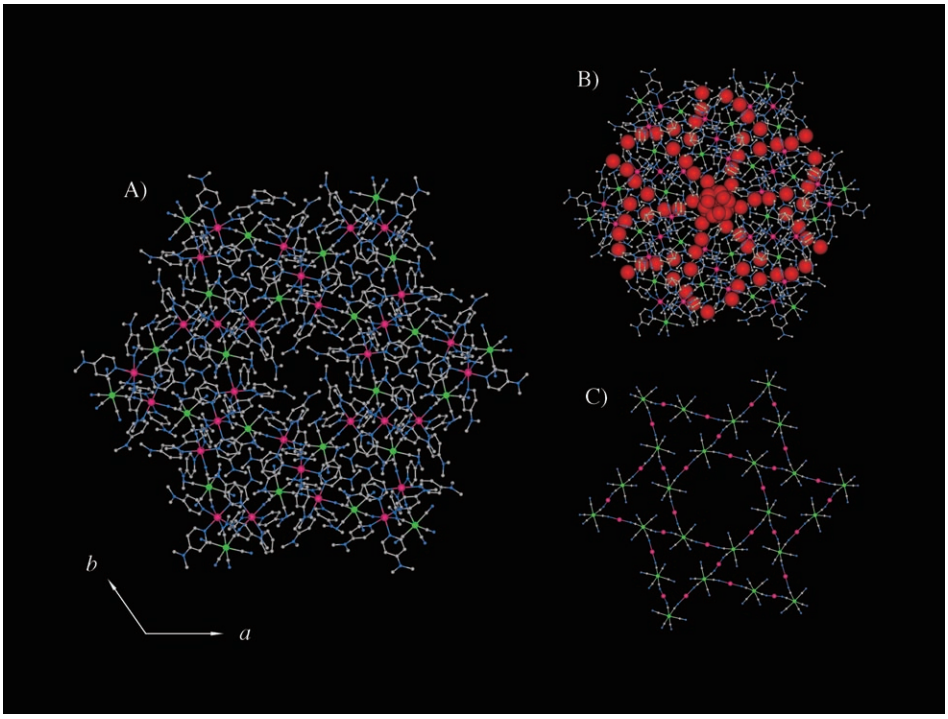

Figure 2. 3D network structure of $[Mn(4dmap)_4]_3[Cr(CN)_6]_2\cdot 10H_2O$ (**1**) without hydrogen atoms and lattice water molecules (A), with lattice water molecules (oxygen atoms are denoted by the red spheres) (B) and without 4dmap molecules (C). Color code: Cr green, Mn pink, N blue, and C gray.

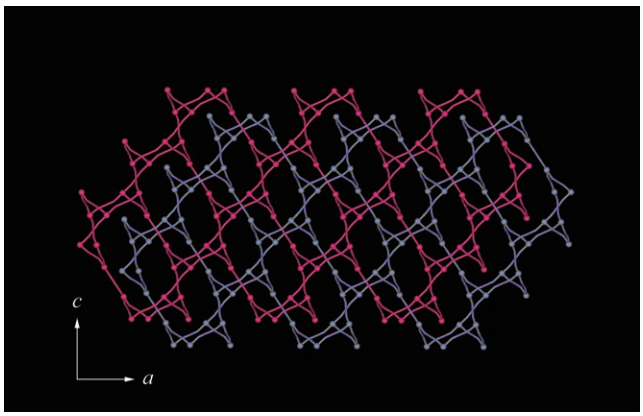

Figure 3. Twofold interpenetrated network of **1**. The topology is represented by the triconnected $6,10^2$ net with Cr^{III} as the nodes (denoted by the spheres) and CN-Mn-NC bonds as the linkers (denoted by the lines). Hydrogen atoms, 4dmap, lattice water, and non-coordinated cyanide groups are omitted for clarity.

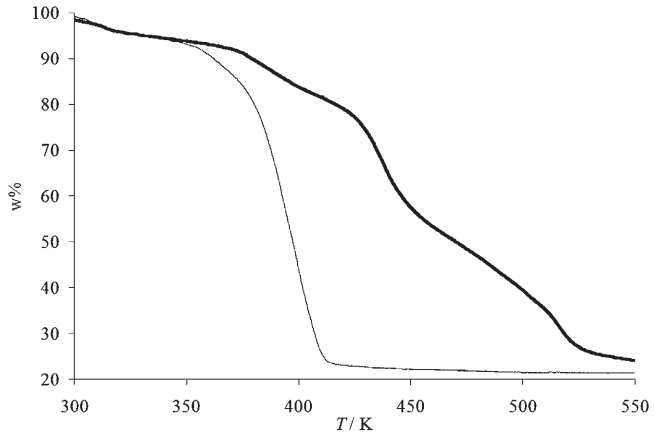

Figure 4. TGA profiles for **1** (thick line) and **2** (thin line).

mally fragile M-CN-Mn linkages, and the differing TGA behavior reflects the stability of the respective $[M(CN)_6]^{3-}$ components. A thermally stable dehydrated state could not be individually prepared, despite many trials under various conditions (see Figure S4 in the Supporting Information), which suggests that the lattice water molecules strongly contribute to the stabilization of the porous framework through hydrogen bonding.

The thermal variation of the XRPD pattern also supports the structural decomposition of **1** and **2** on heating (see Figures S5 and S6 in the Supporting Information). The XRPD patterns of both compounds at room temperature correspond to simulated patterns calculated from the X-ray crystal structures. The peak intensities immediately decreased and broadened on heating. In particular, the (101), (20−1), and (6−4−2) peaks, which are planes including the Mn^{II} centers, notably shifted to higher angles and broadened. The initial patterns were not recovered on being exposed to water vapor with cooling or even on soaking in water.

Magnetic properties: χ_M versus T plots for **1** and **2** in an applied dc field of 500 Oe are shown in Figure 5.

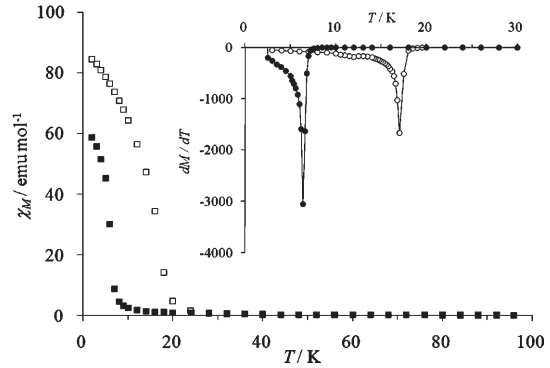

Figure 5. Temperature-dependence of the molar magnetic susceptibility χ_M for **1** (□) and **2** (■) in an applied field of 500 Oe. Inset: dM/dT versus T plots using the field-cooled magnetization data of **1** (○) and **2** (●).

$Mn^{II}_3Cr^{III}_2$ compound (1): The value of χ_M at 300 K per $Mn^{II}_3Cr^{III}_2$ unit was 0.0537 emu mol^{-1} (11.4 μ_B), which corresponds to the spin-only value (0.0563 emu mol^{-1}, 11.6 μ_B) expected for three magnetically isolated Mn^{II} ($S=5/2$) ions and two magnetically isolated Cr^{III} ($S=3/2$) ions. The μ_{eff} value gradually decreased with temperature to a minimum value of 0.180 emu mol^{-1} (9.60 μ_B) at 64 K, and then increased very rapidly below 20 K up to a maximum value of 56.4 emu mol^{-1} (73.6 μ_B) at 12 K (see Figure S7 in the Supporting Information). The $1/\chi_M$ versus T plot in the temperature range of 100–300 K obeys a Curie–Weiss law with a Weiss constant θ of −67 K. The negative value of θ suggests an antiferromagnetic interaction operates between the Mn^{II} and Cr^{III} ions through the cyanide bridges. The rapid increase of the μ_{eff} value below 20 K indicates a long-range ferrimagnetic ordering. The magnetic phase transition temperature, T_C, was determined to be 17.0 K from weak-field magnetization measurements in an applied dc magnetic field of 5 Oe (see Figure S8 in the Supporting Information), the dM/dT differential plot (inset in Figure 5), and from ac magnetic measurements (Figure 6). The in-phase signal (χ_M')

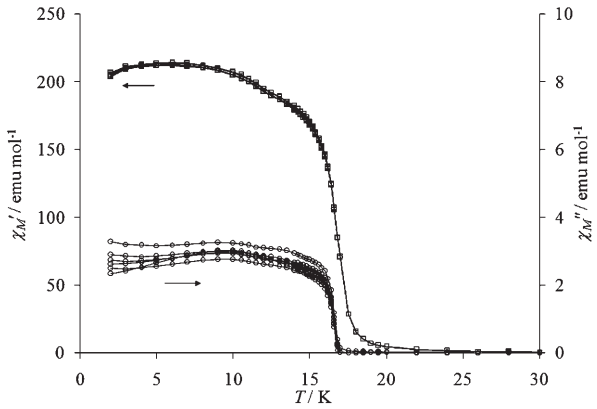

Figure 6. Temperature dependence of the ac magnetic response of **1** in an applied ac field of 3 Oe at frequencies of 1, 5, 10, 50, 100, and 250 Hz.

and the out-of-phase signal (χ_M'') components increased abruptly below 17.0 K, which also defines the value of T_C as 17.0 K.

The T_C is approximately represented by using the molecular field theory as given in Equation (1):[32,33]

$$T_C = 2(n_{Cr}n_{Mn})^{1/2}|J|\{S_{Cr}(S_{Cr}+1)S_{Mn}(S_{Mn}+1)\}^{1/2}/3k_B \qquad (1)$$

where n_i denotes the number of the nearest magnetic center around i ion, J is the exchange interaction constant, S is the spin quantum number, and k_B is Boltzmann's constant. Compared with the corresponding cyanide-bridged $Mn^{II}Cr^{III}$ compounds, the T_C value of **1** is remarkably low; for example, $(n_{Cr}, n_{Mn})=(6, 4)$ and $T_C=63$ K for the related Prussian blue analogue, $Mn_3[Cr(CN)_6]_2\cdot 12H_2O$ (where n_i is an average value),[27,37] $(n_{Cr}, n_{Mn})=(6, 4)$ and $T_C=69$ K for the

three-dimensional complex $[Mn(en)]_3[Cr(CN)_6]_2\cdot 4H_2O$ (en = ethylenediamine),[28] (n_{Cr}, n_{Mn}) = (4, 4) and T_C = 35–38 K for the two-dimensional complex $[Mn(HL)(H_2O)][Cr(CN)_6]\cdot H_2O$ (L = (−)-(*S*)-1,2-diaminopropane, *N*,*N*-dimethylethylenediamine),[29,31] whereas (n_{Cr}, n_{Mn}) = (3, 2) and T_C = 17 K for **1**. The decrease in both n_{Cr} and n_{Mn} is the major reason for the notable decrease in T_C. On the other hand, J is approximately defined as the product of the intranet interaction (J_{intra}) and the internet interaction (J_{inter}); for example, $|J| = (|J_{intra}||J_{inter}|^2)^{1/3}$ for a 1D system, $(|J_{intra}|^2|J_{inter}|)^{1/3}$ for a 2D system, and $|J_{intra}|$ for an ideal 3D system. In the case of an interpenetrated 3D system, a weak internet interaction would give rise to a small contribution to the value of T_C.[11,12] Although, in general, $|J_{inter}|$ is much smaller than $|J_{intra}|$, the J_{inter} value is the dominant factor for magnetic ordering in a low-dimensional system.

Besides the ferrimagnetic transition at 17 K, a minor minimum was observed at 12 K in the dM/dT differential plot. The zero field-cooled magnetization and χ_M'' signals also showed an inflection point around 11 K. The anomaly appearing around 12 K was attributed to the coexistence of a partially dehydrated compound, because the intensity of the minor peak was dependent on the sample, and **1** easily loses some of its lattice water molecules under low humidity conditions.

The field-dependence of the magnetization at 2 K is shown in Figure 7. The M versus H curve showed a high gradient increase and became saturated below 1 kOe. The saturation magnetization value per $Mn^{II}{}_3Cr^{III}{}_2$ unit at 50 kOe was 8.73 $N\beta$, which corresponds to the value of S = 9/2 expected for three antiferromagnetically coupled Mn^{II} ions and two antiferromagnetically coupled Cr^{III} ions. The theoretical curve based on the Brillouin function for S = 9/2 (g = 1.96) is shown as the solid line in Figure 7. The M versus H curve demonstrates the ferrimagnetic ordering. The magnetic hysteresis loop at 2 K is shown in the inset in Figure 7. The residual magnetization and coercive field were close to zero, which means that **1** is a typical soft magnet because of the isotropic electronic configuration of the Mn^{II} and Cr^{III} ions, and the symmetrical 3D network topology.

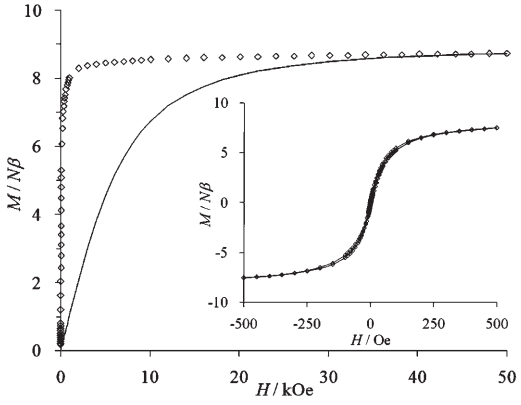

Figure 7. Field-dependence of the magnetization of **1** at 2 K. The solid line denotes the Brillouin function for S = 9/2 using g = 1.96. The inset shows the hysteresis loop measured at 2 K. The solid line is for guidance only.

$Mn^{II}{}_3Mn^{III}{}_2$ compound (2): The value of χ_M at 300 K per $Mn^{II}{}_3Mn^{III}{}_2$ unit was 0.0524 emu mol^{-1} (11.2 μ_B), which corresponds to the spin-only value (0.0504 emu mol^{-1}, 11.0 μ_B) expected for three magnetically isolated Mn^{II} (S = 5/2) ions and two low-spin Mn^{III} (S = 2/2) ions (Figure 5). The μ_{eff} value gradually diminished with decreasing temperature down to a minimum value of 0.267 emu mol^{-1} (10.1 μ_B) at 48 K, and then rapidly increased below 20 K up to a maximum value of 45.1 emu mol^{-1} (42.5 μ_B) at 5 K (see Figure S9 in the Supporting Information). This behavior also indicates ferrimagnetic ordering. A Curie–Weiss plot in the temperature range of 100–300 K gave a negative Weiss constant of θ = −25 K, which reflects an antiferromagnetic interaction operating between the Mn^{II} and Mn^{III} ions through the cyanide bridges and a spin-orbit coupling of the low-spin Mn^{III} ions (ground state $^3T_1$).

The T_C value was determined to be 6.4 K from weak field magnetization measurements under 5 Oe (see Figure S10 in the Supporting Information), a dM/dT differential plot (inset Figure 5), and from ac magnetic susceptibility measurements (Figure 8). Compared with the corresponding cyanide-bridged $Mn^{II}Mn^{III}$ compounds, the T_C value of **2** was also remarkably low for the same reason as discussed for **1**; for example, ($n_{Mn(III)}$, $n_{Mn(II)}$) = (6, 4) and T_C = 37 K for the related Prussian blue analogue, $Mn_3[Mn(CN)_6]_2\cdot xH_2O$ (n_i is an average value),[38,39] ($n_{Mn(III)}$, $n_{Mn(II)}$) = (4, 4) and T_C = 21 K for $[Mn(HL)(H_2O)][Mn(CN)_6]\cdot H_2O$ (L = (−)-(*S*)- or (+)-(*R*)-1,2-diaminopropane),[31] whereas ($n_{Mn(III)}$, $n_{Mn(II)}$) = (3, 2) and T_C = 6.4 K for **2**.

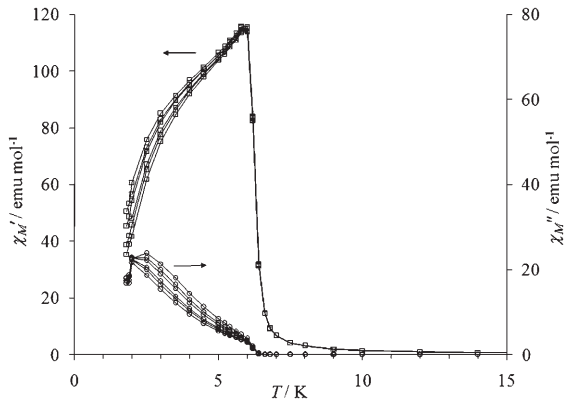

Figure 8. Temperature dependences of the ac magnetic response of **2** in an applied ac field of 3 Oe at frequencies of 1, 5, 10, 50, 100, and 250 Hz.

Below T_C, the χ_M' signal rapidly decreased, which is a different behavior from that of **1**. This difference reflects the magnetic anisotropy of the Mn^{III} ions, which hardens the magnetic domain structure. In addition, the ac response showed a small frequency dependence below T_C. The secon-

dary anomaly that appeared around 11 K in **1** was also observed around 3 K in **2**.

The value of T_C and $|\theta|$ for **2** were lower than those of **1**. A similar trend was confirmed in the 2D cyanide-bridged ferrimagnets $[Mn(HL)(H_2O)][M(CN)_6]\cdot H_2O$ (L = 1,2-diaminopropane, $T_C = 38$ K for $M = Cr^{III}$ and 21 K for Mn^{III}), which was explained by considering the electronic configuration and magnetic orbitals of the M^{III} ions.[29,31] The exchange interaction constant, J_{ex}, was described by $(9|J_{AF}| + 6|J_F|)/15$ for **1** and $(6|J_{AF}| + 4|J_F|)/10$ for **2**, where J_{AF} and J_F denote the magnitude of the antiferromagnetic and the ferromagnetic interaction between each unpaired electron, respectively. In the case of the low-spin Mn^{III}, $|J_{AF}|$ was smaller than the magnetically isotropic Cr^{III} ion because of the different electronic distribution of the $[M(CN)_6]^{3-}$ unit in the pseudo C_{2v} symmetric environment and the contribution of the spin-orbit coupling, which is applicable to the case of the low-spin Fe^{III} ion. In addition, the mixed valence $Mn^{II}Mn^{III}$ compound **2** potentially provides a ferromagnetic contribution based on the double exchange interaction.[42] These factors give negative contributions to both J_{ex} and T_C in **2**.

The field-dependence of the magnetization at 2 K of **2** is shown in Figure S11 in the Supporting Information, with the Brillouin function for $S = 11/2$ ($g = 2.04$) shown by the solid line. The value of M increased rapidly below 500 Oe, and then gradually increased up to 50 kOe. The magnetization value per $Mn^{II}_3Mn^{III}_2$ unit at 50 kOe was 11.1 $N\beta$, which corresponds to the expected value of $S = 11/2$. The high gradient of the M versus H curve in the low magnetic field region demonstrated the ferrimagnetic ordering in the bulk, and the gradual increase with an inflection point above 500 Oe reflected the magnetic anisotropy of the Mn^{III} ions. A typical magnetic hysteresis loop was observed at 2 K (see Figure S11 in the Supporting Information). Compared with **1**, the remnant magnetization (2.5×10^4 emu Oe mol^{-1}) and the coercive field (400 Oe) of **2** were higher, because of the contribution of the magnetic anisotropy of the incorporated Mn^{III} ions instead of the magnetically isotropic Cr^{III} ions in **1**.[29,31,43]

Effect of pressure on the magnetic properties: The static magnetic susceptibility of **1** and **2** under various hydrostatic pressures (up to 1.0 GPa) is shown in Figure 9 and Figure S13 in the Supporting Information in the form of M versus T plots, where M is the magnetization value per sample mass (ca. 5 mg). The hydrostatic pressure was applied by using a piston-cylinder type of pressure cell employing Apiezon grease J as a pressure-transmitting medium, and the effective pressure at low temperature was calibrated by using the superconducting transition of Pb.[44–48] The magnetization of Pb vanished on applying a dc magnetic field of 1 kOe (critical field at $T = 0$ is ca. 0.8 kOe). In both **1** and **2**, the reversibility in the magnetic behavior was confirmed by releasing pressure after successive measurements up to 1.0 GPa.

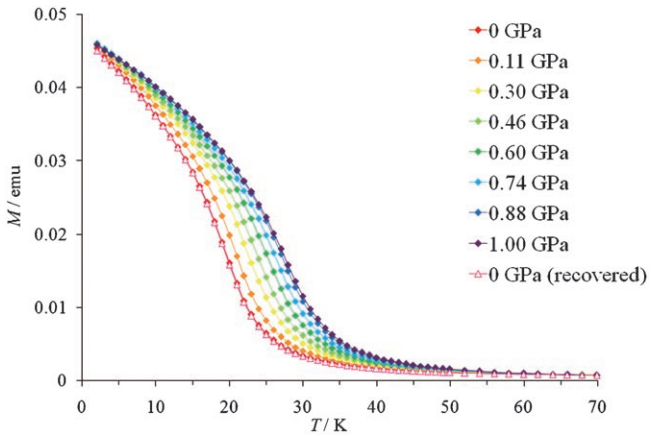

Figure 9. Temperature dependence of the magnetization (M) of **1** at various hydrostatic pressures.

The M versus T curve of **1** under ambient pressure corresponds to the χ_M versus T curve shown in Figure 5. It gradually shifted towards higher temperatures with increasing pressure. The value of T_C under pressure was determined from the ac magnetic measurements in an ac field of 3 Oe and frequency of 10 Hz (Figure 10 and Figure S12 in the

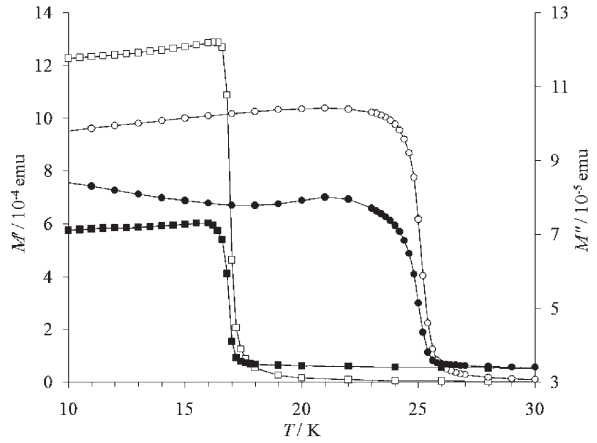

Figure 10. Temperature dependences of the in-phase and the out-of-phase magnetization (M'(open) and M''(closed)) of **1** in an ac field of 3 Oe at a frequency of 10 Hz, under ambient pressure (square) and 1.00 GPa (circle), respectively.

Supporting Information). The value of T_C at 0 GPa was 17.0 K and this increased to 25.4 K at 1.00 GPa. The pressure dependence of T_C is shown in Figure 11, which clearly demonstrates the linear relationship of T_C with the applied pressure, with $dT_C/dP = 8.43$ K/GPa (see Figure S15 in the Supporting Information). When the pressure was released at 1.00 GPa, the M–T curves traced back to the initial profile, and the T_C value recovered to 17.0 K. These results indicate a reversible T_C modulation without any structural decomposition under an external pressure up to 1.00 GPa. The precise T_C modulation resulting from the external pressure re-

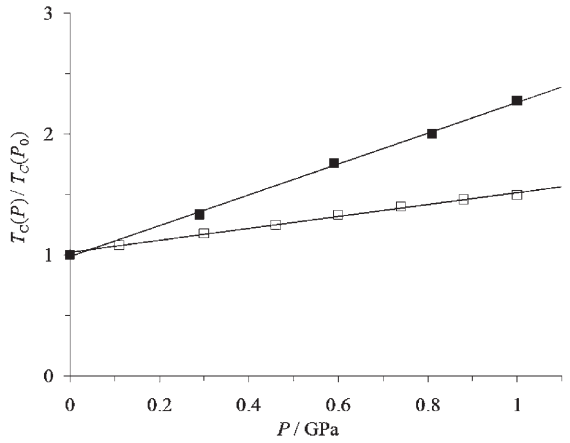

Figure 11. Pressure dependences of $T_C(P)/T_C(P_0)$ of **1** (open squares) and **2** (closed squares).

flects the increased overlap integrals between $d\pi(Cr^{III})$ and $\pi^*(CN^-)$ and between $d\pi(Mn^{II})$ and $\pi^*(CN^-)$ orbitals, accompanied by a shrinkage of the Cr-CN-Mn linkages.[48] The maximum magnetization value at 2 K was constant for all pressures, which suggests that the magnetic domain structure was not changed under stress. The internet interaction was negligible in the initial interpenetrated structure, because the nearest internet separation of 10.646 Å (between the nearest Cr^{III} and Cr^{III} ions) was enough long. In this case, the internet interaction is weakly ferromagnetic based on the dipolar interaction and might be enhanced on application of external pressure.[11,12] However, in practice, the contribution of the internet interaction is not so large, because the bulky 4dmap coligands separate the two independent nets well, and prevent shrinkage of the internet space. In addition, the constant magnetization value at 2 K indicates that there was no pressure-induced linkage isomerism of the cyanide groups in **1** at pressures up to 1.00 GPa, while this phenomenon has been reported in other Prussian-blue analogues.[50]

A similar T_C enhancement associated with applying an external pressure was observed in **2** (see Figure S13–15 in the Supporting Information). The T_C value of **2** increased to 15.0 K at 1.04 GPa, with a linear correlation of $dT_C/dP =$ 8.41 K/GPa. The applied pressure makes the antiferromagnetic pathway including magnetically anisotropic Mn^{III} ions more effective. To elucidate the origin of the T_C enhancement more directly, structural analysis of both **1** and **2** under an applied external pressure is in progress.

Here we compare the rates of T_C change of **1**, **2** and previously reported CPMs, and discuss the effect of pressure. The rate of T_C change (the initial slope a) in the small P region can be estimated by Equation (2):[47]

$$T_C(P) = (1 + aP) \times T_C(P_0) \quad (2)$$

where $T_C(P_0)$ is T_C under ambient pressure.

In the case of **1**, the initial slope a is estimated to be 0.49 GPa^{-1}, where $T_C(P_0) = 17.0$ K and $T_C(1.00) = 25.4$ K (Figure 11). With **2**, a is estimated to be 1.29 GPa^{-1} ($T_C(P_0) = 6.4$ K and $T_C(1.04) = 15.0$ K).

The effect of pressure on CPMs, $[Mn(en)]_3[Cr(CN)_6]_2 \cdot 4H_2O$ (**3**), $Mn_3[Mn(CN)_6]_2 \cdot 12H_2O \cdot 1.7CH_3OH$ (**4**), and $Co_5(OH)_6(SO_4)_2(H_2O)_4$ (**5**) have already been reported.[30,48,49] Compound **3** has a 3D network based on a defective cubane structure extended by Cr^{III}-CN-Mn^{II} linkages with (n_{Cr}, n_{Mn}) = (6, 4), and the $T_C(P_0)$ value of 69 K increased up to 102 K at 1.36 GPa, which gives an a value of 0.35 GPa^{-1}. Prussian-blue analogue **4** shows an increase of T_C from 29 K to 40 K at 1.00 GPa, where the a value is estimated to be 0.38 GPa^{-1}. Compound **5** forms a 3D pillared layer structure based on μ_3-OH-bridged Co^{II} layers and $[Co^{II}(H_2O)_4(SO_4)_2]$ pillars, and gives an a value of 0.097 GPa^{-1} ($T_C(P_0) = 12.6$ K and $T_C(0.98) = 13.8$ K). The results are summarized in Table 1. The a value can be treated as a measure of the compressibility of the structure with regard to its magnetic properties. The low a value of **5** reflects its structural hardness and its well-separated 2D magnetic structure. The cyanide-bridged CPMs, **3** and **4**, give comparable a values. Compared with $Mn^{II}Cr^{III}$ ferrimagnets **1** and **3**, the higher a value (higher compressibility) of **1** is consistent with its flexible porous framework. It should be noted that the a value of **2** is remarkably higher than that of **1** in spite of the same flexible framework. The high a value of **2** suggests that the magnetic interaction pathway including magnetically anisotropic Mn^{III} ions in the C_{2v} symmetry was made more effective by structural compression. The a values of **1** and **2** are also comparable or higher than those of compound **6** having a 1D alternate array of $[M(hfac)_2]$ (Hhfac = hexafluoroacetylacetone) and chiral α-nitronyl nitroxide radical ((*R*)-3MLNN) with ferromagnetic ordering ($T_C(P_0) = 4.7$ K, $T_C(0.98) = 5.7$ K in 120 Oe),[51] and a pure organic weak ferromagnet, β-phase of 1,2,3,5-Dithiadiazol-3-yl,4-(4-cyano-2,3,5,6-tetrafluorophenyl) radical (p-NCC_6F_4CNSSN (**7**)), providing the highest T_C value of genuine organic magnet ($T_C(P_0) = 36$ K, $T_C(1.64) = 72$ K) (Table 1).[46,47] In the interpenetrating flexible porous magnets **1** and **2**, the spatial margin between frameworks plays an important role for the high compression.

Table 1. T_C and initial slope a of compounds **1**–**7**.

Compound	$T_C(P_0)$ [K]	$T_C(P)$ [K]	(P [GPa])	a [GPa^{-1}]
$[Mn(4dmap)_4]_2[Cr(CN)_6]_3 \cdot 10H_2O$ **1**	17.0	25.4	(1.00)	0.49
$[Mn(4dmap)_4]_2[Mn(CN)_6]_3 \cdot 10H_2O$ **2**	6.4	15.0	(1.04)	1.29
$[Mn(en)]_3[Cr(CN)_6]_2 \cdot 4H_2O$ **3**	69	102	(1.36)	0.35
$Mn_3[Mn(CN)_6]_2 \cdot 12H_2O \cdot 1.7CH_3OH$ **4**	29	40	(1.00)	0.38
$Co_5(OH)_6(SO_4)_2(H_2O)_4$ **5**	12.6	13.8	(0.98)	0.097
(*R*)-3MLNN-$Mn(hfac)_2$ **6**	4.7	5.7	(0.98)	0.22
p-NCC_6F_4CNSSN **7**	36	72	(1.64)	0.61

Conclusion

Two novel 3D cyanide-bridged ferrimagnets, $[Mn(4dmap)_4]_3[M(CN)_6]_2\cdot 10H_2O$ (M = Cr (**1**) and Mn (**2**)) have been prepared by using monodentate 4dmap as a coligand. Both compounds form a twofold interpenetrated 3D network based on triconnected $6,10^2$ nets with M^{III} nodes and CN-Mn^{II}-NC linkers. The frameworks exhibit porosity with two types of 1D basic channels, and these channels are filled with lattice water molecules. The compounds exhibit a ferrimagnetic ordering (T_C = 17.0 K (**1**) and 6.4 K (**2**)) at ambient pressure, and a reversible T_C modulation on applying an external hydrostatic pressure. The value of T_C increased linearly to 25.4 K for **1** and 15.0 K for **2** on applying pressure up to 1.0 GPa. This is because of the enhancement of the antiferromagnetic interaction by structural compression associated with an increase in the overlap integral between the magnetic orbitals of M^{III} and Mn^{II} ions. The frameworks also provided chemically modified inner pores with the basic dimethylamino groups. Such modification of porous coordination polymers (PCPs) is an intriguing subject, because it has a crucial effect on guest adsorption, separation, and catalytic reactions in the specific coordination space.[52–55] In addition, interpenetrating porous frameworks are significant in that they exhibit guest-induced functions because of their dynamic coordination space.[2–5,56–61] Compounds **1** and **2** demonstrate an advantage for attaining multifunctionality, such as physical (pressure) and chemical (guest molecules) responsive magnets, except for their instability towards dehydration. The preparation of such materials, providing interpenetrated rigid magnetic frameworks and a specific inner space, is in progress to achieve multifunctionality based on reversible physical and/or chemical responses.

Experimental Section

Physical measurements: Elemental analyses of carbon, hydrogen, and nitrogen were carried out on a Flash EA 1112 series, Thermo Finnigan instrument. Infrared spectra were measured by using KBr disks with a PerkinElmer Spectrum 2000 FT-IR system. Variable-temperature X-ray powder diffraction was collected on a Rigaku RINT 2000 Ultima diffractometer with $Cu_{K\alpha}$ radiation. Thermogravimetric analyses were recorded on a Rigaku Thermo plus TG 8120 apparatus in the temperature range between 300 and 700 K under a nitrogen atmosphere at a heating rate of 1 K min^{-1}. The ac and dc magnetic susceptibility measurements under an ambient pressure were carried on a Quantum Design MPMS-XL5R SQUID magnetometer in the temperature range 2–300 K. Crystals of **1** and **2** were well ground and mixed into the commercially available Apiezon J Oil (Apiezon Products M&I Materials Ltd, UK) to fix the sample and to avoid the dehydration under a He atmosphere (low humidity) during the measurement. The respective mixture was placed in a gelatin capsule, mounted inside a straw, and fixed to the end of a sample transport rod. Effective magnetic moments were calculated by applying the equation $\mu_{eff}=(8\chi_M T)^{1/2}$, where χ_M is the molar magnetic susceptibility corrected for diamagnetism of the constituting atoms.[62] Field-dependences of magnetization were measured under the field range of 0–50 kOe. The magnetic measurements under a hydrostatic pressure up to 1.04 GPa were carried out by using a piston-cylinder type of pressure cell made of Cu-Be alloy, which can be inserted into a SQUID magnetometer. Apiezon J oil was used as a pressure-transmitting medium. The sample (5–10 mg) was well ground and dispersed into the apiezon oil with a piece of Pb, whose superconducting transition temperature served as the probe of the actual pressure at low temperature. The mixture was placed in the Teflon bucket and fixed in the clamp cell.[44–47]

Materials: All reagents except for $K_3[Mn(CN)_6]$ were purchased from commercial sources and used without further purification. $K_3[Mn(CN)_6]$ was prepared according to the literature.[63] All preparations were carried out under anaerobic conditions (Ar flow) using standard Schlenk apparatus and degassed solvents to avoid oxidation by atmospheric dioxygen. **Caution**: Cyanide-containing compounds are potentially toxic and should be handled in small quantities.

Preparations

$[Mn(4dmap)_4]_3[Cr(CN)_6]_2\cdot 10H_2O$ (1): $MnCl_2\cdot 4H_2O$ (59 mg, 0.3 mmol) was dissolved in a degassed water–ethanol (2:1) solution (10 mL). A water–ethanol (2:1) solution (10 mL) of 4dmap (220 mg, 1.8 mmol) and that of $K_3[Cr(CN)_6]$ (65 mg, 0.2 mmol) were added to this solution in turn. The resulting turbid mixture was allowed to stand for over two weeks to obtain pale green cubic crystals. They were separated, collected by suction filtration, washed with water, and dried in vacuo. All the operations for the synthesis were carried out in the dark to avoid the decomposition of $K_3[Cr(CN)_6]$. Yield: 169 mg (76%). Elemental analysis (%) calcd for $C_{96}H_{140}N_{36}O_{10}Cr_2Mn_3$: C 51.77, H 6.34, N 22.64; found: C 51.61, H 6.11, N 22.40. Selected FT-IR data(KBr disk): $\tilde{\nu}$ = 2156, 2131 cm^{-1} (ν_{CN}).

$[Mn(4dmap)_4]_3[Mn(CN)_6]_2\cdot 10H_2O$ (2): This compound was synthesized in a way similar to that for **1** except for using $K_3[Mn(CN)_6]$ (65 mg, 0.2 mmol), a different amount of 4dmap (147 mg, 1.2 mmol), and degassed water as solvent at 276 K instead of $K_3[Cr(CN)_6]$, 4dmap (220 mg, 1.8 mmol) and the water–ethanol mixture at room temperature. The resulting turbid mixture was allowed to stand for a week to obtain resulting reddish-brown cubic crystals. They were separated, collected by suction filtration, washed with water, and dried in vacuo. All the operations for the synthesis were carried out under cold condition in the dark to avoid the decomposition of $K_3[Mn(CN)_6]$. Yield: 168 mg (75%). Elemental analysis (%) calcd for $C_{96}H_{140}N_{36}O_{10}Mn_5$: C 51.63, H 6.32, N 22.58; found: C 51.39, H 6.01, N 22.63. Selected FT-IR data(KBr disk): $\tilde{\nu}$ = 2141, 2135, 2120, 2118 cm^{-1} (ν_{CN}).

X-ray crystallography: The data of **1** and **2** were collected on a RIGAKU/MSC Mercury diffractometer to a maximum 2θ value of 55.0° with graphite-monochromated $Mo_{K\alpha}$ radiation (λ = 0.71070 Å). A total of 720 oscillation images were collected. The data sets were recorded as ω scans at 0.3° steps and the exposure rate was 180.0 (s/°). An absorption correction based on the crystal shape was applied. The data were corrected for Lorentz and polarization effects. The structure was solved by direct methods and expanded by using Fourier techniques. Non-hydrogen atoms were refined anisotropically, while hydrogen atoms were placed at calculated positions and refined isotropically. All calculations were performed by using the teXsan crystallographic software package of Molecular Structure Corporation.[64]

Crystal data for $[Mn(4dmap)_4]_3[Cr(CN)_6]_2\cdot 10H_2O$ (1) at 243 K: A pale green cubic crystal, $C_{96}H_{140}N_{36}O_{10}Cr_2Mn_3$, FW = 2227.20, crystal size 0.30 × 0.25 × 0.25 mm, space group $R\bar{3}$ (No. 148), Z = 9, $a = b$ = 38.759(9), c = 20.559(5) Å, $\alpha = \beta$ = 90°, γ = 120°, V = 26747.2(8) Å^3, ρ_{calcd} = 1.244 g cm^{-3}, $\mu(Mo_{K\alpha})$ = 5.53 cm^{-1}. The refinement converges with R = 0.062, R_w = 0.046 for 8352 reflections ($I > 0.7\sigma(I)$, F^2) and R_1 = 0.032 for $I > 2.0\sigma(I)$.

Crystal data for $[Mn(4dmap)_4]_3[Mn(CN)_6]_2\cdot 10H_2O$ (2) at 243 K: A reddish-brown block crystal, $C_{96}H_{140}N_{36}O_{10}Mn_5$, FW = 2233.09, crystal size 0.15 × 0.12 × 0.13 mm, space group $R\bar{3}$ (No. 148), Z = 9, $a = b$ = 38.46(1), c = 20.287(6) Å, $\alpha = \beta$ = 90°, γ = 120°, V = 25982(12) Å^3, ρ_{calcd} = 1.284 g cm^{-3}, $\mu(Mo_{K\alpha})$ = 6.00 cm^{-1}. The refinement converges with R = 0.116, R_w = 0.089 for 5478 reflections ($I > 0.7\sigma(I)$, F^2) and R_1 = 0.045 for $I > 2.0\sigma(I)$.

CCDC-658663 and CCDC-658664 contain the supplementary crystallographic data for this paper. These data can be obtained free of charge

from the Cambridge Crystallographic Data Centre via www.ccdc.cam.ac.uk/data_request/cif.

Acknowledgements

This work was supported by a Grant-In-Aid for Science Research in a Priority Area 'Chemistry of Coordination Space (No. 16074209)', a Grant-In-Aid for Scientific Research Program (No. 18750046), and CREST/JST program from the Ministry of Education, Culture, Sports, Science, and Technology of Japan. W. K. is grateful to JSPS Research Fellowships for Young Scientists.

[1] O. Sato, T. Iyoda, A. Fujishima, K. Hashimoto, *Science* **1996**, *272*, 704–705.
[2] E. Coronado, J. R. Galán-Mascarós, C. J. Gómez-García, V. Laukhin, *Nature* **2000**, *408*, 447–449.
[3] D. Maspoch, D. Ruiz-Molina, K. Wurst, N. Domingo, M. Cavalliano, F. Biscarini, J. Tejada, C. Rovira, J. Veciana, *Nat. Mater.* **2003**, *2*, 190–195.
[4] V. Niel, A. L. Thompson, M. C. Muñoz, A. Galet, A. E. Goeta, J. A. Real, *Angew. Chem.* **2003**, *115*, 3890–3893; *Angew. Chem. Int. Ed.* **2003**, *42*, 3760–3766.
[5] H. Cui, Z. Wang, K. Takahashi, Y. Okano, H. Kobayashi, A. Kobayashi, *J. Am. Chem. Soc.* **2006**, *128*, 15074–15075.
[6] S. Kitagawa, R. Kitaura, S-i. Noro, *Angew. Chem.* **2004**, *116*, 2388–2430; *Angew. Chem. Int. Ed.* **2004**, *43*, 2334–2375.
[7] K. Nakatani, P. Bergerat, E. Codjovi, C. Mathoniere, Y. Pei, O. Kahn, *Inorg. Chem.* **1991**, *30*, 3977–3978.
[8] S. Turner, O. Kahn, L. Rabardel, *J. Am. Chem. Soc.* **1996**, *118*, 6428–6432.
[9] H. Miyasaka, N. Matsumoto, N. Re, E. Gallo, H. Ôkawa, *Inorg. Chem.* **1997**, *36*, 670–676.
[10] J. Larionova, S. A. Chavan, J. V. Yakhmi, A. G. Frøystein, J. Sletten, C. Sourisseau, O. Kahn, *Inorg. Chem.* **1997**, *36*, 6374–6381.
[11] M. Ohba, H. Ôkawa, N. Fukita, Y. Hashimoto, *J. Am. Chem. Soc.* **1997**, *119*, 1011–1019.
[12] M. Drillon, P. Panissod, *J. Mag. Mag. Mater.* **1998**, *188*, 93–99.
[13] H. Miyasaka, H. Ieda, N. Matsumoto, N. Re, R. Crescenzi, C. Floriani, *Inorg. Chem.* **1998**, *37*, 255–263.
[14] N. Usuki, M. Ohba, H. Ôkawa, *J. Bull. Chem. Soc. Jpn.* **2002**, *75*, 1693–1698.
[15] D. Maspoch, D. Ruiz-Molina, J. Veciana, *Chem. Soc. Rev.* **2007**, *36*, 770–818.
[16] S. Ohkoshi, K. Arai, Y. Sato, K. Hashimoto, *Nat. Mater.* **2004**, *3*, 857–860.
[17] Z. Wang, B. Zhang, H. Fujiwara, H. Kobayashi, M. Kurmoo, *Chem. Commun.* **2004**, 416–417.
[18] M. Kurmoo, H. Kumagai, K. W. Chapman, C. J. Kepert, *Chem. Commun.* **2005**, 3012–3014.
[19] S. Ohkoshi, Y. Tsunobuchi, H. Takahashi, T. Hozumi, M. Shiro, K. Hashimoto, *J. Am. Chem. Soc.* **2007**, *129*, 3084–3085.
[20] N. Yanai, W. Kaneko, K. Yoneda, M. Ohba, S. Kitagawa, *J. Am. Chem. Soc.* **2007**, *129*, 3496–3497.
[21] W. Kaneko, M. Ohba, S. Kitagawa, *J. Am. Chem. Soc.* **2007**, *129*, 13706–13712.
[22] O. Kahn, *Molecular Magnetism*, VCH, Weinheim, **1993**.
[23] K. R. Dunbar, R. A. Heintz, *Prog. Inorg. Chem.* **1997**, *45*,283–391.
[24] M. Ohba, H. Ôkawa, *Coord. Chem. Rev.* **2000**, *198*, 313–328.
[25] H. Ôkawa, M. Ohba, *Bull. Chem. Soc. Jpn.* **2002**, *75*, 1191–1203.
[26] M. Ohba, N. Maruono, H. Ôkawa, T. Enoki, J.-M. Latour, *J. Am. Chem. Soc.* **1994**, *116*, 11566–11567.
[27] N. Usuki, M. Yamada, M. Ohba, H. Ôkawa, *J. Solid State Chem.* **2001**, *159*, 328–335.
[28] M. Ohba, N. Usuki, N. Fukita, H. Ôkawa, *Angew. Chem.* **1999**, *111*, 1911–1914; *Angew. Chem. Int. Ed.* **1999**, *38*, 1795–1798.
[29] K. Inoue, K. Kikuchi, M. Ohba, H. Ôkawa, *Angew. Chem.* **2003**, *115*, 4958–4961; *Angew. Chem. Int. Ed.* **2003**, *42*, 4810–4813.
[30] T. Maeda, M. Mito, H. Deguchi, S. Takagi, W. Kaneko, M. Ohba, H. Ôkawa, *Polyhedron* **2005**, *24*, 2497–2500.
[31] W. Kaneko, S. Kitagawa, M. Ohba, *J. Am. Chem. Soc.* **2007**, *129*, 248–249.
[32] L. Néel, *Annals Phys.* **1948**, *3*, 137–198.
[33] J. L. Manson, C. Campana, J. S. Miller, *Chem. Commun.* **1998**, 251–252.
[34] J. S. Miller, *Adv. Mater.* **2001**, *13*, 525–527.
[35] T. E. Vos, Y. Liao, W. Shum, J-H. Her, P. W. Stephens, W. M. Reiff, J. S. Miller, *J. Am. Chem. Soc.* **2004**, *126*, 11630–11639.
[36] K. Nakamoto, *Infrared and Raman Spectra of Inorganic and Coordination Compounds*, 5th ed, Wiley, New York, **1997**.
[37] D. Babel, *Comments Inorg. Chem.* **1986**, *5*, 285–320.
[38] W. R. Entley, G. S. Girolani, *Inorg. Chem.* **1994**, *33*, 5165–5166.
[39] W. R. Entley, G. S. Girolani, *Inorg. Chem.* **1995**, *34*, 2262.
[40] A. F. Wells, *Three-dimensional nets and polyhedra*, Wiley, New York, **1977**.
[41] A. L. Spek, *PLATON, a multipurpose crystallographic tool*, Utrecht University, Utrecht, The Netherlands, **2001**.
[42] C. Zener, *Phys. Rev.* **1951**, *81*, 403–405.
[43] E. Ruiz, A. R- Fortea, S. Alvarez, M. Verdaguer, *Chem. Eur. J.* **2005**, *11*, 2135–2144.
[44] A. Eiling, J. S. Schilling, *J. Phys.* **1981**, *11*, 623–639.
[45] Y. Hosokoshi, M. Tamura, M. Kinoshita, *Mol. Cryst. Liq. Cryst.* **1997**, *306*, 423–430.
[46] M. Mito, T. Kawae, K. Takeda, S. Takagi, Y. Matsushita, H. Deguchi, J. M. Rawson, F. Palacio, *Polyhedron* **2001**, *20*, 1509–1512.
[47] K. Takeda, M. Mito in *Carbon-Based Magnetism*, (Eds. T. Makarova, F. Palacio), Elsevier B. V., **2006**, 131–158.
[48] K. Awaga, T. Sekine, M. Okawa, W. Fujita, S. M. Holmes, G. S. Girolami, *Chem. Phys. Lett.* **1998**, *293*, 352–356.
[49] M. B. Salah, S. Vilminot, G. André, M. Richard-Plouet, T. Mhiri, S. Takagi, M. Kurmoo, *J. Am. Chem. Soc. J. Am Chem. Soc.* **2006**, *128*, 7972–7981.
[50] E. Coronado, M. C. Giménez-López, G. Levchenko, F. M. Romero, V. García-Baonza, A. Milner, M. Paz-Pasternak, *J. Am. Chem. Soc.* **2005**, *127*, 4580–4581.
[51] V. Laukhin, B. Martínes, J. Fontcuberta, D. B. Amabilino, M. Minguet, J. Veciana, *J. Phys. Chem. B* **2004**, *108*, 18441–18445.
[52] J. S. Seo, D. Whang, H. Lee, S. I. Jun, J. Oh, Y. J. Jeon, K. Kim, *Nature* **2006**, *404*, 982–986.
[53] R. Matsuda, R. Kitaura, S. Kitagawa, Y. Kubota, T. C. Kobayashi, S. Horike, M. Takata, *J. Am. Chem. Soc.* **2004**, *126*, 14063–14070.
[54] M. P. Suh, J. W. Ko, H. J. Choi, *J. Am. Chem. Soc.* **2006**, *128*, 4710–4718.
[55] S. Hasegawa, S. Horike, R. Matsuda, S. Furukawa, K. Mochizuki, Y. Kinoshita, S. Kitagawa, *J. Am. Chem. Soc.* **2007**, *129*, 2607–2614.
[56] R. Kitaura, K. Seki, G. Akiyama, S. Kitagawa, *Angew. Chem.* **2003**, *115*, 444–447; *Angew. Chem. Int. Ed.* **2003**, *42*, 428–431.
[57] K. Uemura, S. Kitagawa, K. Fukui, K Saito, *J. Am. Chem. Soc.* **2004**, *126*, 3817–3828.
[58] S-H. Cho, B. Ma, S. T. Nguyen, J. T. Hupp, T. E Albrecht-Schmitt, *Chem. Commun.* **2006**, 2563–2565.
[59] T. K. Maji, R. Matsuda, S. Kitagawa, *Nat. Mater.* **2007**, *6*, 142–148.
[60] G. J. Halder, C. J. Kepert, B. Moubaraki, K. S. Murray, J. D. Cashion, *Science* **2002**, *298*, 1762–1765.
[61] C. J. Kepert, *Chem. Commun.* **2006**, 695–700.
[62] E. A. Boudreaux, L. N. Mulay, *Theory and Applications of Molecular Paramagnetism*, Wiley, New York, **1976**.
[63] J. Meyer, *Z. Anorg. Chem.* **1913**, *81*, 385–405.
[64] teXsan: Crystal Structure Analysis Package, The Molecular Structure Corporation, Woodlands, TX (**1985** & **1999**).

Received: August 30, 2007
Published online: February 18, 2008

